alone. However, all of the model simulations, which used global SST anomalies, did produce these (Fig. 1, B and D). It is likely that the model responses in these regions are the result of extratropical anomalies. Results from a subsequent suite of numerical experiments performed to separate the effects of various tropical and extratropical SST anomalies also suggest this connection.

This investigation does not preclude the possibility that the observed warming of the tropical oceans is the end result of global warming itself. If so, our results imply that the spatial and temporal characteristics of the global warming trends are manifested as a bias in the frequency of occurrence of one of the modes of the natural variability of the ocean-atmosphere system, that is, ENSO. As a corollary, the AGCMs that do not simulate these modes of natural variability for the present climate may also misrepresent the spatial and temporal characteristics of predicted global warming.

REFERENCES AND NOTES

1. M. S. Halpert and C. H. Ropelewski, *J. Clim.* **5**, 577 (1992).
2. M. L. Blackmon, J. E. Geisler, E. J. Pitcher, *J. Atmos. Sci.* **40**, 1410 (1983).
3. N. C. Lau, *Mon. Weather Rev.* **113**, 1970 (1985).
4. L. Bengtsson *et al.*, *Science* **261**, 1026 (1993).
5. M. Ji, A. Kumar, A. Leetmaa, *Tellus A* **46**, 398 (1994).
6. M. Kanamitsu, *Weather Forecast.* **4**, 335 (1989).
7. R. W. Reynolds, *J. Clim.* **1**, 75 (1988).
8. For the source of observed surface temperature-data, see C. F. Ropelewski, J. E. Janowiak, M. S. Halpert, *Mon. Weather Rev.* **113**, 1101 (1985).
9. J. T. Houghton, B. A. Callander, S. K. Varney, Eds., *Climate Change: The Supplementary Report to the IPCC Scientific Assessment* (Cambridge Univ. Press, Cambridge, 1992).
10. The model error for the ENSO composite in the tropical eastern hemisphere can also be seen in the comparison of Fig. 1, A and B.
11. J. D. Horel and J. M. Wallace, *Mon. Weather Rev.* **109**, 813 (1981).
12. M. P. Hoerling *et al.*, *J. Clim.* **5**, 669 (1992).
13. J. D. Opsteegh and H. M. Van den Dool, *J. Atmos. Sci.* **37**, 2169 (1980).
14. Conclusions similar to this have been obtained in an observational study by K. E. Trenberth and J. W. Hurrell [*Clim. Dyn.* **9**, 303 (1994)].
15. Support provided by National Oceanic and Atmospheric Administration's office of Global Programs through the Climate and Global Change Program is gratefully acknowledged.

23 May 1994; accepted 7 September 1994

Causes of Decadal Climate Variability over the North Pacific and North America

M. Latif* and T. P. Barnett

The cause of decadal climate variability over the North Pacific Ocean and North America is investigated by the analysis of data from a multidecadal integration with a state-of-the-art coupled ocean-atmosphere model and observations. About one-third of the low-frequency climate variability in the region of interest can be attributed to a cycle involving unstable air-sea interactions between the subtropical gyre circulation in the North Pacific and the Aleutian low-pressure system. The existence of this cycle provides a basis for long-range climate forecasting over the western United States at decadal time scales.

The origins of decadal climate variability over the North Pacific Ocean and North America, characterized by anomalous surface temperatures and surface pressures (*1–4*), are uncertain. A recent example of the impact of such decadal climate variability is the multiyear drought over the southwestern United States. It has been speculated by some researchers that unstable air-sea interactions over the North Pacific and changes in the large-scale ocean circulation might force the decadal climate variability (*5, 6*), while other studies suggest that tropical forcing is a stronger influence (*2, 4, 7*). In this report, we develop a consistent physical picture of how decadal climate variability over the North Pacific and North America may be generated.

To study the decadal climate variability, we used a state-of-the-art coupled model of global ocean-atmosphere general circulation (ECHO) (*8*), which was forced by seasonally varying insolation and integrating for 70 years. The coupled model simulates well the mean climate and observed short-term interannual variability. In particular, it simulates realistically the El Niño–Southern Oscillation (ENSO) phenomenon. An earlier version of this model was also applied successfully to predict the behavior of ENSO (*9*). The coupled model simulates pronounced decadal variability over the North Pacific and North America during the course of the 70-year integration. One example (Fig. 1A) of such variability is the anomalous sea surface temperature (SST) in the western Pacific in the region of the Kuroshio extension. Simulated SSTs in this region exhibit a distinct irregular oscillatory behavior on a decadal time scale, with maximum anomalies of slightly less than 1°C. There are three manifestations of the decadal mode.

To determine the spatial coherence of the decadal-scale SST variability, we computed the associated SST regression pattern (Fig. 1B). It is dominated by a large-scale positive SST anomaly centered near 35°N and extending from the Asian coast almost across the entire Pacific. The orientation of this positive anomaly coincides approximately with the position of the model Kuroshio current and its eastward extension. The positive SST anomaly is surrounded by negative anomalies, most prominently in the south. The space-time structure of the SST anomalies can be represented as a combination of a standing wave pattern and a propagating pattern, with the latter component dominating in the region of the Kuroshio and its extension. The spatial structure of the SST anomalies affects the meridional temperature gradient in the Pacific, which has important consequences for

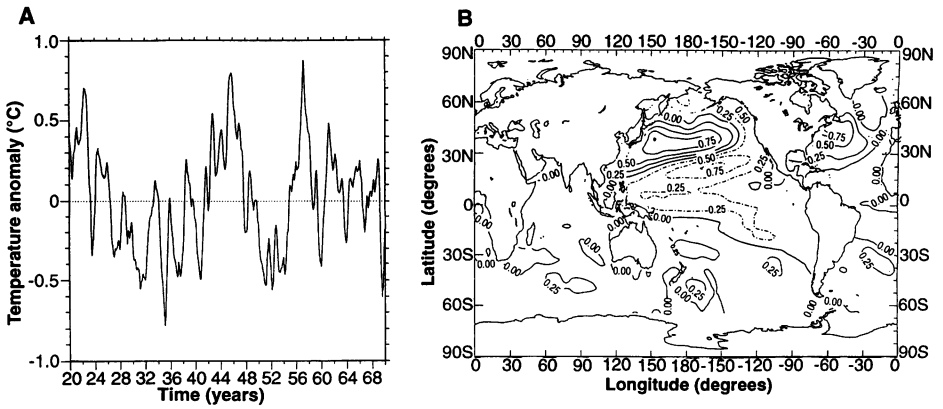

Fig. 1. (**A**) Time series of the coupled model's anomalous SST (°C) averaged over the region from 150°E to 180°E and 25°N to 35°N. The time series was smoothed with a 9-months running mean filter. (**B**) Spatial distribution of linear regression coefficients between the index time series shown in (A) and SST values. The pattern was scaled so that the maximum SST anomalies were to 1°C.

M. Latif, Max-Planck-Institut für Meteorologie, Bundestrasse 55, D-20146 Hamburg, Germany.
T. P. Barnett, Climate Research Division, Scripps Institution of Oceanography, La Jolla, CA 92093–0224, USA.
*To whom correspondence should be addressed.

the atmospheric circulation.

To elucidate the mechanism producing the SST pattern, we investigated the characteristic evolution of upper-ocean heat content anomalies, as defined by the vertically averaged temperatures over the upper 500 m of the water column by using a complex empirical orthogonal function (CEOF) analysis (*10*). Before the CEOF analysis, the heat content data were smoothed with a low-pass filter that retained variability at time scales of more than 3 years. The leading CEOF mode, accounting for about one-third of the variance in the filtered heat content data, has a period of about 20 years. Anomalies in upper-ocean heat content reconstructed from this leading CEOF mode (Fig. 2) are displayed at intervals of about 2.5 years. When the SST anomalies are fully developed and in a stage corresponding to that shown in Fig. 1B, the main heat-content anomaly is positive and covers the majority of the western and Central Pacific (Fig. 2, upper panel). A negative anomaly extends southwesterly from North America and increases in area and strength as it approaches the tropics. With time, through one-half of a cycle, the large anomalies rotate around the Pacific in a clockwise fashion reminiscent of the general gyral circulation. Thereafter, the whole sequence of events is repeated but with reversed signs, which completes one full cycle.

This evolution is characteristic of the transient response of a mid-latitude ocean to a variable wind stress, as described in many theoretical and modeling papers [for example, (*11–13*)]. The response is mostly baroclinic at climate time scales of more than several months and involves the propagation of long, relatively fast planetary waves with westward group velocity and their reflection into short, relatively slow planetary waves with eastward group velocity. However, the mean horizontal currents affect the wave propagation. The net effect of this wave propagation is to modify the strength of the subtropical gyre circulation (*13*). In particular, resultant fluctuations in the poleward transport of warm tropical waters by

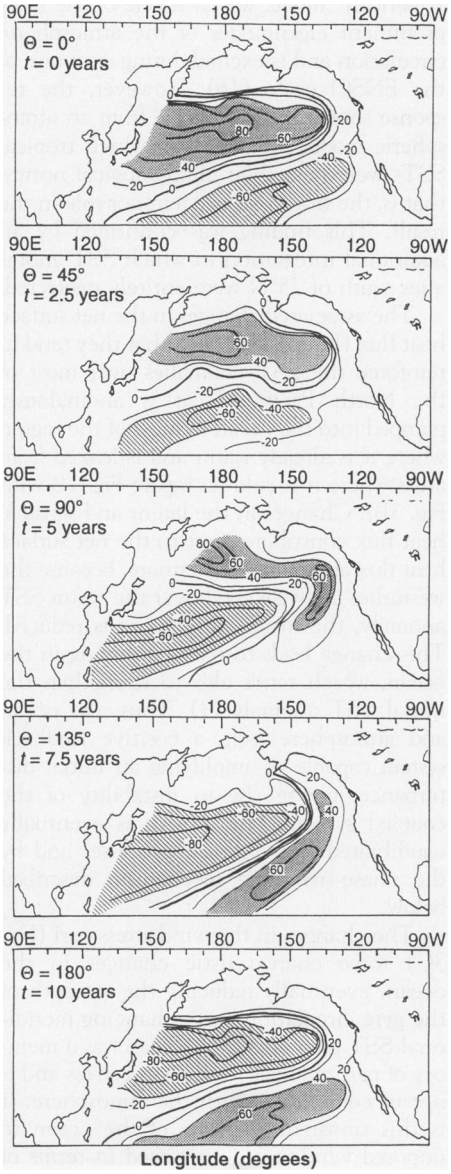

Fig. 2. Reconstruction of anomalous heat content (degrees Celsius · meters) from the leading CEOF mode. The individual panels show the heat content anomalies at different stages of the decadal cycle, approximately 2.5 years apart. The phase angle Θ measures the phase of cycle (full cycle = 360°).

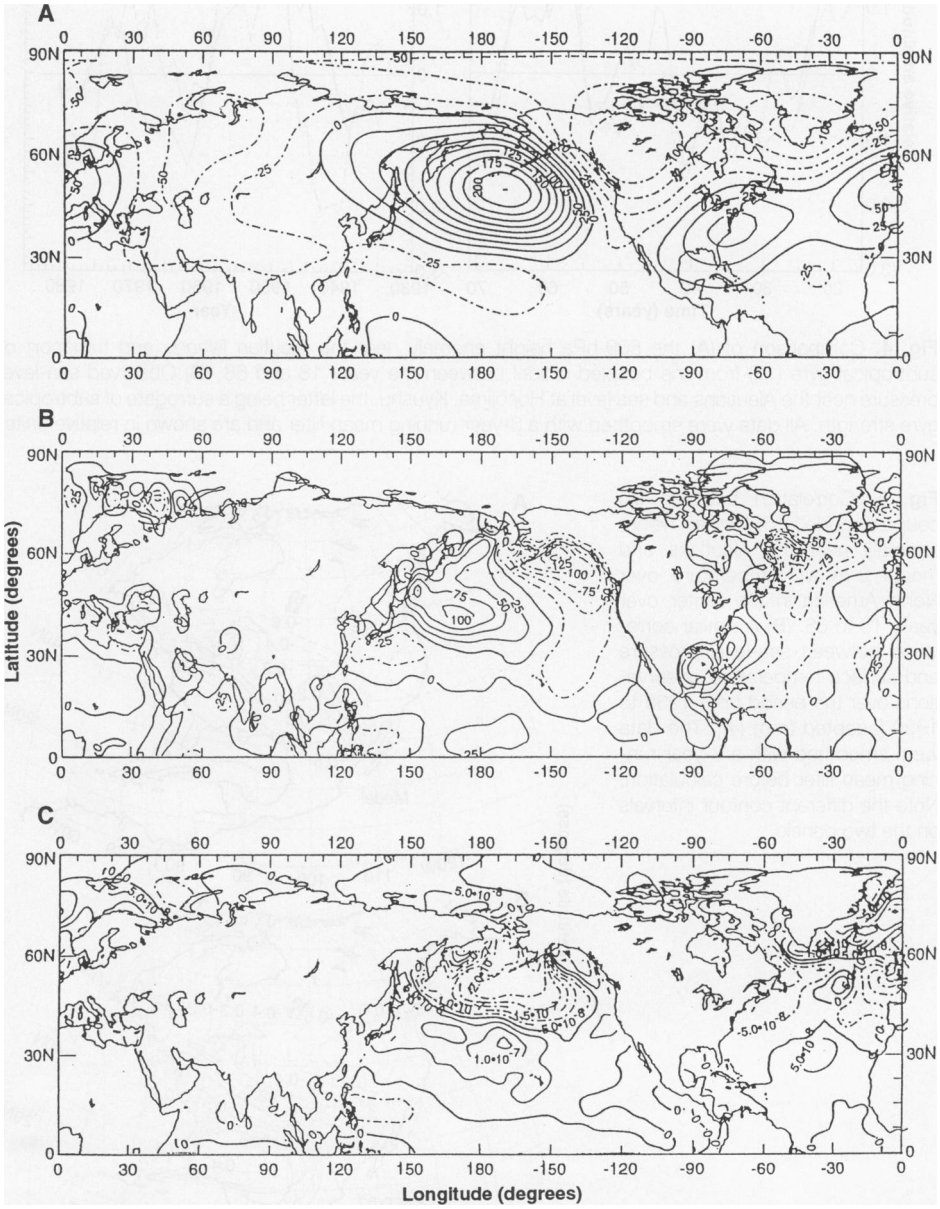

Fig. 3. Atmospheric response to the SST anomaly shown in Fig. 1B. (**A**) The response in the 500-hPa field (geopotential meters). (**B**) The net surface heat flux (watts per square meter). (**C**) The wind stress curl (pascals per meter). The mean fields shown in the panels were obtained by averaging the results of a 12-member ensemble of 30-day perpetual January integrations with the use of the same SST forcing.

the western boundary current lead to the generation of SST anomalies along the path of the Kuroshio and its extension. The spin-up time of the subtropical gyre, of which the changes in the western boundary current are a part, is several years to a decade or more, which accounts for the decadal time scale of the mode under discussion.

The remaining task is to explain the oscillatory nature of this mode. Our hypothesis is that it arises from an instability of the coupled ocean-atmosphere system in the North Pacific. The characteristic SST anomaly pattern exhibits a strong meridional gradient that either reduces or enhances the meridional SST gradient normally found in the Central Pacific.

Suppose the coupled system is in its reduced meridional SST gradient state (Fig. 1B). It has been suggested (*14*) that such a distribution of SST would result in a northward shift of the baroclinic eddy activity in the atmosphere, leading to a weakened Aleutian low and subsequently reduced westerly winds over the mid-latitudes ocean. Indeed, the model results show that a reduced meridional SST gradient is accompanied by anomalous high pressure over the entire North Pacific.

To investigate further the nature of the atmospheric response to the anomalous SST pattern, we forced the atmospheric component of our coupled model in a stand-alone integration by the SST pattern shown in Fig. 1B. The integration was done in a perpetual January mode, and an ensemble of 12 January integrations was performed. The atmospheric response is highly significant and shows the expected result: anomalous high pressure over the North Pacific (Fig. 3A) (*15*). The response pattern is the weak Aleutian-low extreme of the "Pacific North American" mode, which is one of the most prominent eigenmodes of the atmospheric circulation and is excited during extremes of the ENSO cycle (*16*). However, the response shown in Fig. 3 arose from an atmospheric model simulation in which tropical SSTs were near their climatological norms; that is, the tropics played a minor role in the result. This finding was confirmed by an additional integration in which SST anomalies south of 25°N were entirely neglected.

The associated changes in the net surface heat flux (Fig. 3B) are such that they tend to reinforce the SST anomalies over most of the North Pacific. Heat is anomalously pumped into the ocean in most of the region where it is already warm and is leaked from areas where it is cold (compare Fig. 1B with Fig. 3B). Changes in the latent and sensible heat flux contribute most to the net surface heat flux anomaly. Furthermore, because the westerlies are weakened over the warm SST anomaly, the mean wind speed is reduced. This change leads to reduced mixing in the ocean, which tends also to strengthen the initial SST anomaly (*3*). Thus, the ocean and atmosphere form a positive feedback system capable of amplifying an initial disturbance, giving rise to instability of the coupled system. The growth is eventually equilibrated by nonlinear processes and by the phase-switching mechanism described below.

The changes in the wind stress curl (Fig. 3C) force characteristic changes in the ocean, eventually reducing the strength of the gyre circulation and enhancing meridional SST gradients. The ocean has a memory of past changes in the wind stress and is not in equilibrium with the atmosphere. It is this transient response of the ocean to imposed wind stress, expressed in terms of planetary wave propagation (Fig. 2), that causes a change from one phase of the decadal mode to another and, hence, enables the coupled system to oscillate. The oscillation can easily become irregular in the presence of high-frequency weather

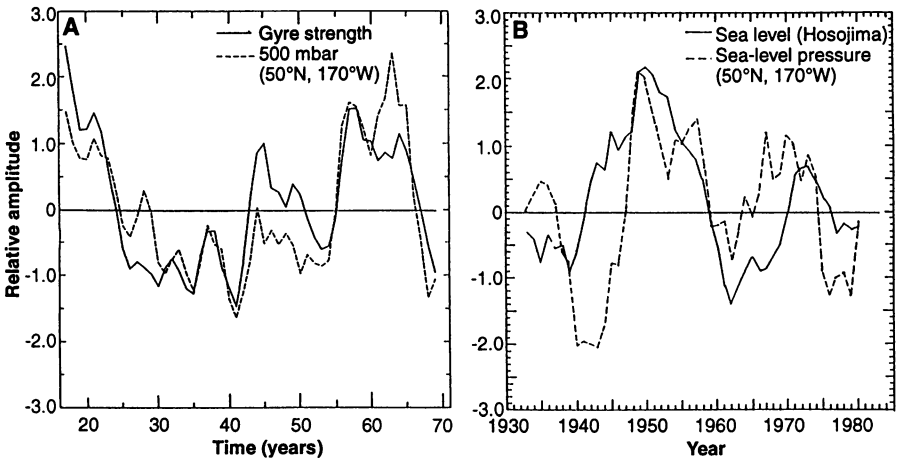

Fig. 4. Comparison of (**A**) the 500-hPa height anomaly near the Aleutian Islands and transport of subtropical gyre (*17*) from the coupled model between the years 18 and 68. (**B**) Observed sea-level pressure near the Aleutians and sea level at Hosojima, Kyushu, the latter being a surrogate of subtropical gyre strength. All data were smoothed with a 3-year running mean filter and are shown in relative units.

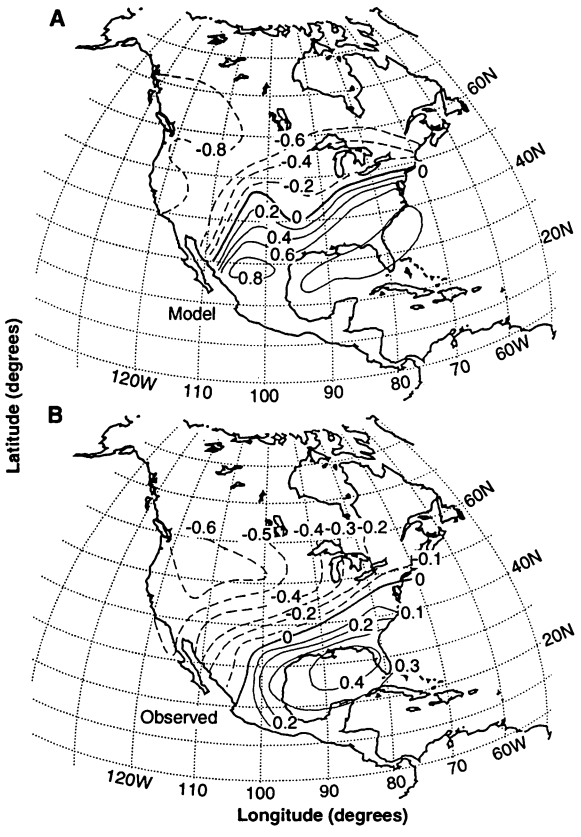

Fig. 5. Correlation between (**A**) coupled-model, 500-hPa height anomaly near the Aleutians and model 2-m air temperature over North America in the winter over years 18 to 68. (**B**) A similar correlation between sea-level pressure and surface-temperature observations over the period from 1935 to 1990 [adapted from (*4*)]. The data were smoothed with a 3-year running mean filter before calculation. Note the different contour intervals on the two panels.

fluctuations. Some elements of these ideas were suggested over 20 years ago (*5*, *6*).

The model results are observable in the real world. For instance, SST patterns and their associated atmospheric patterns, as determined from observations (*1*, *2*, *4*), are close to those from our simulation. Further, projection of the last 45 years of observed SST fields onto the leading EOF of the anomalous SST field from the model yielded a principal component whose amplitude and characteristic time scale closely resemble those of the principal component of the model. More important, the relation between atmospheric response and ocean transport indices was the same in the model and in observations (*17*): Gyre strength and atmospheric pressure vary in phase on decadal time scales (Fig. 4).

North Atlantic SST variability exhibits pronounced energy at time scales of about 10 years (*18*). This pattern is consistent with our scenario, because the zonal width of the North Atlantic is only about half that of the North Pacific. Moreover, the spatial patterns of the decadal variability observed in the North Atlantic region agree with those we found in the North Pacific region: Anomalously warm SSTs and anomalously high pressure occur together and the associated changes in the surface heat flux and oceanic mixing tend to reinforce the SST anomalies (*18*).

Both the model and observations show a strong, simultaneous wintertime relation between low-pass filtered anomalies of atmospheric pressure in the heart of the main atmospheric response region south of the Aleutians (Fig. 3) and air temperature over North America (Fig. 5) (*1*, *4*, *19*). The remarkable accuracy of the model in reproducing the dipole correlation over North America suggests that it can be used to forecast decadal climate change numerically over North America (*20*). At a minimum, knowledge of the present phase of the Pacific mode obtained from current observational programs should allow a "nowcast" (*21*) of expected climate "bias" associated with this decadal climate change, which is equivalent to a climate forecast of several years in the future.

REFERENCES AND NOTES

1. J. Namias, *J. Geophys. Res.* **64**, 631 (1959); *Mon. Weather Rev.* **97**, 173 (1969).
2. N. E. Graham, *Clim. Dyn.* **10**, 135 (1994).
3. A. J. Miller *et al.*, *ibid.* **9**, 287 (1994).
4. K. E. Trenberth and J. W. Hurrell, *ibid.*, p. 303.
5. J. Bjerknes, *Advances in Geophysics* (Academic Press, New York, 1964), pp. 1–82.
6. W. B. White and T. P. Barnett, *J. Phys. Oceanogr.* **2**, 372 (1972).
7. G. A. Jacobs *et al.*, *Nature* **370**, 360 (1994).
8. M. Latif *et al.*, *Tellus A* **46**, 351 (1944). The atmospheric component is the standard Max-Planck-Institut (MPI) model ECHAM3, while the oceanic component is the Hamburg Ocean Model in Primitive Equations (HOPE) model, a primitive equation model of global ocean dynamics also developed at MPI. Both models have a resolution of approximately 2.5° by 2.5° in mid-latitudes. The resolution of the ocean model, however, is higher in the tropics. The ocean and atmosphere interact within the region from 60°N to 60°S, without the application of any flux correction. Poleward of 60°, SST and salinity are relaxed to the climatology by the use of a Newtonian formulation.
9. M. Latif, A. Sterl, E. Maier-Reimer, M. M. Junge, *J. Clim.* **6**, 700 (1993).
10. T. P. Barnett, *Mon. Weather Rev.* **111**, 756 (1983).
11. D. L. T. Anderson and A. E. Gill, *Deep Sea Res.* **22**, 583 (1975).
12. D. L. T. Anderson, K. Bryan, A. E. Gill, R. C. Pacanowski, *J. Geophys. Res.* **84**, 4795 (1979).
13. A. E. Gill, *Atmosphere-Ocean Dynamics* (Academic Press, New York, 1982), pp. 507–512.
14. T. N. Palmer and Z. Sun, *Q. J. R. Meteorol. Soc.* **111**, 947 (1985); N.-C. Lau and M. J. Nath, *J. Clim.* **3**, 965 (1990); Y. Kushnir and N.-C. Lau, *ibid.* **5**, 271 (1992); L. Ferranti, F. Molteni, T. N. Palmer, *Q. J. R. Meteorol. Soc.*, in press.
15. Typical decadal-scale 500-hPa height anomalies over the North Pacific simulated by the coupled model are on the order of about 10 geopotential meters.
16. J. D. Horel and J. M. Wallace, *Mon. Weather Rev.* **109**, 813 (1981).
17. The ocean transport index from the model is the meridional gradient of the density field in the upper 500 m at the dateline. An index of the Kuroshio strength (and, hence, the gyre) was taken to be the observed sea level at Hosojima, Kyushu, Japan.
18. C. Deser and M. L. Blackmon, *J. Clim.* **6**, 1743 (1993).
19. T. P. Barnett, *Mon. Weather Rev.* **109**, 1021 (1981).
20. The long-range (decadal) forecasts would require that the ocean component of the coupled model be initialized with at least the observed thermal structure of the upper 500 m of the Pacific over a region extending from the Aleutians to 20°N and from Asia to North America. Existing expendable bathythermograph and buoy programs are close to providing the required information.
21. This phrase was coined by J. J. O'Brien (Florida State University).

22. We thank D. Cayan and W. White for many fruitful discussions; N. Schneider and D. Pierce for providing suggestions on an earlier version of the manuscript; and T. Stockdale, J. Wolff, and E. Maier-Reimer for helping to develop the coupled model; we also thank the Theoretical Applications Division of the Los Alamos National Laboratory for making most of the computer time available for these runs; D. Poling for tending these runs and managing the extensive output files; and C. Keller for facilitating the cooperation on this project. In addition, we thank M. Junge, J. Ritchie, T. Tubbs, and M. Tyree for providing computational assistance. Supported in part by the National Science Foundation under grant NSFATM 9314495, the U.S. Department of Energy's CHAMP program under grant DE-FG03-91-ER61215 (T.P.B.), the German Climate Computer Center (DKRZ), and the European Community under grant EV5V-CT92-0121 (M.L.).

27 June 1994; accepted 30 August 1994

Middle Cambrian Arthropod Embryos with Blastomeres

Xi-guang Zhang and Brian R. Pratt

A phosphatized Middle Cambrian (~510 million years ago) fauna from Duyun, southern China, has yielded fossil embryos that may be of arthropod affinity and could belong to the co-occurring eodiscid trilobite *Pagetia* sp. The shell was most likely flexible and possessed at least two thin layers. Four embryos reveal blastomeres, and two embryonic stages are represented. These embryos demonstrate that the basic paradigm for the growth of the invertebrate embryo has not changed in more than half a billion years.

A unicellular zygote (fertilized egg) is converted into a multicellular organism by successive cleavages during embryonic development. Lacking mineralized tissues, however, invertebrate eggs are unlikely to escape breakdown. Fossil examples are therefore exceedingly scarce, and none reveal embryonic stages. Among the Echinodermata, for instance, only a single blastoid from the Lower Pennsylvanian of Oklahoma contains probable eggs (*1*). Fossil trilobite eggs were mentioned in several 19th-century publications but were not conclusive (*2*). The trilobite embryo and the suspected preprotaspis stage have been unknown (*3*). Possible ostracode eggs from the Lower Cambrian of China (*4*) and Lower Cretaceous of Brazil (*5*), as well as shrimp eggs similarly from the Cretaceous of Brazil (*6*), are nondescript spheres (*7*). Possible Middle Cretaceous insect eggs from Brazil (*8*) have not been substantiated, but a single, Upper Cretaceous moth eggshell from Massachusetts does possess a well-preserved lepidopteran sculpture (*9*). In this report, we describe fossil eggs that contain embryos bearing delicate blastomeres.

Department of Geological Sciences, University of Saskatchewan, Saskatoon, Saskatchewan S7N 0W0, Canada.

These embryos are phosphatized and co-occur with many trilobite juveniles (protaspides and meraspides) of the eodiscid *Pagetia* sp. and an unidentified polymeroid trilobite, a few adult bradoriid ostracodes, and lots of inarticulate brachiopod valves. We liberated these fossils by dilute (~5%) acetic acid digestion of 7 kg of a thin, bioclastic limestone bed sandwiched between gray dolomites within the lower part of the Middle Cambrian Gaotai Formation in Duyun, Guizhou, China.

The five embryos are ovoid (Figs. 1 and 2). The lengths range from 0.30 to 0.35 mm, and the widths from 0.24 to 0.27 mm (*10*). The shell, being about 1.5 μm thick and